# Electronic correlations of element cerium under high pressure

Haiyan Lu1,2 and Li Huang1,\*

<sup>1</sup>Science and Technology on Surface Physics and Chemistry Laboratory, P.O. Box 9-35, Jiangyou 621908, China

<sup>2</sup>Beijing National Laboratory for Condensed Matter Physics,
and Institute of Physics, Chinese Academy of Sciences, Beijing 100190, China

(Dated: January 4, 2017)

The electronic structures of element cerium under high pressure remain unclear all the time. We tried to calculate the electronic structures of  $\alpha'$ ,  $\alpha''$ , and  $\epsilon$ -Ce which only exist in the presence of pressure, by using the combination of traditional density functional theory and single-site dynamical mean-field theory. The momentum-resolved band structures, total and partial density of states, 4f electronic configurations of these phases were exhaustively studied. We found that the 4f electrons tend to be itinerant, and the hybridizations between the 4f and spd conduction electrons are remarkable. In addition, the fluctuations among the 4f atomic eigenstates are prominent, especially for the  $\epsilon$  phase, which leads to a slight modification of its 4f occupancy.

### PACS numbers: 71.10.-w, 71.27.+a, 71.30.+h, 74.20.Pq

## I. INTRODUCTION

Ce is one of the most mysterious elements in the periodic table because of its unusual electronic structures which manifest in its multiple allotropic phases. Under ambient pressure, Ce may exhibit four allotropes  $(\alpha, \beta, \gamma, \text{ and } \delta \text{ phases})$ , and undergo three successive solid phase transitions before reaching its liquid state [1]. When  $P \sim 0.8$  GPa and at room temperature, strikingly, an iso-structural phase transition would take place between the  $\alpha$  and  $\gamma$  phases (both phases are in facecentered-cubic structure). Though the crystal structure is preserved during the transition, the atomic volume changes by  $\sim$ 15% which has not been observed in any other simple metals. The underlying physics and driving force of the  $\alpha - \gamma$ phase transition have been, and are being to this day, warmly debated. Particularly, concerning the role played by the correlated 4f electrons in the transition, it is still a matter of dispute and ongoing research [2–8].

Besides, under moderate pressure and temperature Ce will exhibit another three distinct phases, namely, the  $\alpha'$ ,  $\alpha''$ , and  $\epsilon$ phases (see Fig. 1), which result in an extremely complicated P-T phase diagram [9]. The crystal structure of the  $\alpha'$  phase is orthorhombic (space group Cmcm). Noted that it is isostructural with  $\alpha$ -U. The  $\alpha''$  phase is monoclinic (space group  $C_2/m$ ). The  $\alpha$ -Ce will transform into the two phases in the pressure range from 5 to 12 GPa, but which phase transition (i.e.,  $\alpha - \alpha'$  or  $\alpha - \alpha''$  transition) could occur in a cerium sample strongly depends on the method of sample preparation. Upon further volume compression (P > 12 GPa) both the  $\alpha'$  and  $\alpha''$  phases can transform into the  $\epsilon$  phase, which is body centered tetragonal (space group  $I_4/mmm$ ). Recently, the inelastic X-ray scattering experiment has demonstrated that there exist strong electron-phonon coupling and pronounced phonon anomalies in the  $\alpha'$  phase, which means that it is at the verge of lattice instability [10]. Similar to  $\alpha$ -U, a charge density wave perhaps develops in the  $\alpha'$ -Ce. Furthermore, the superconductivity with  $T_c \sim 2$  K found in the high-pressure phases

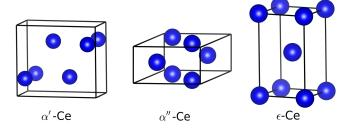


FIG. 1. (Color online). Schematic picture for the crystal structures of  $\alpha'$ ,  $\alpha''$ , and  $\epsilon$ -Ce.

of Ce can be attributed to the  $\alpha'$  phase as well.

It is very difficult to prepare and identify pure high-pressure phases of Ce, which requires precise controls of pressure and thermal process [11]. Therefore, it is not easy to conduct extensively experimental researches. On the other hand, lowsymmetry crystal structures, strong spin-orbit coupling, and notable electronic correlations in 4f electrons also pose great challenges to the first-principles calculations [1]. As a result, though numerous efforts have been made to explore the basic properties of Ce under pressure, actually we know a little about the electronic structures of its high-pressure phases and there are a lot of puzzles that need to be solved. For instance, do the 4f electrons remain itinerant or localized state [12]? What's the consequence in electronic structures since the interplay of spin-orbit coupling and 4f electronic correlations? Are there strong hybridization between the 4f and spd bands as predicted by the Kondo volume collapse (KVC) scenario [4, 5]? Last, but by no means least, are the 4f electronic configurations for these high-pressure phases the same, and are they similar to or different from those for the other phases under ambient pressure [13–19]? In order to answer the above questions, more experimental investigations and theoretical calculations are highly desired.

Bearing these questions in mind, the purpose of this paper is to endeavour to build an unified picture for the evolution of electronic structures of high-pressure phases of Ce, by utilizing the state-of-the-art first-principles many-body approach. The rest of the paper is organized as follows. In Sec. II, we

<sup>\*</sup> Corresponding author: lihuang.dmft@gmail.com

briefly introduce the calculation method and parameters. In Sec. III, we present all of the calculated results and make a detailed discussion. We also compare the 4f electronic configurations between the high-pressure phases and  $\alpha$ -Ce. Finally, Section IV serves as a short summary and conclusion.

#### II. METHODS

In the present work, we employed the density functional theory in combination with the single-site dynamical meanfield theory (dubbed as DFT + DMFT) to study the electronic structures of  $\alpha'$ ,  $\alpha''$ , and  $\epsilon$ -Ce. This approach can treat the strong 4f electronic correlations, spin-orbit coupling as well as on-site Kondo screening on the same footing, and incorporate them into realistic band structures based on DFT calculations. As for the basic principles and technical details of the DFT + DMFT method, please refer to the good reviews (see Refs. [20] and [21]) and references therein. In fact, it is considered as the most powerful method established so far for the calculations of electronic structures of strongly correlated materials, and has been successfully applied to study many interesting problems in lanthanides and actinides, such as the best known  $\alpha - \gamma$  phase transition in Ce [13–19], the low-temperature hidden order phase of URu<sub>2</sub>Si<sub>2</sub> [22], and the valence state fluctuations in Yb [23] and Pu [24, 25].

We performed charge fully self-consistent DFT + DMFT calculations by using the EDMFTF software package [26]. The Kohn-Sham equation within the DFT part was solved by using the WIEN2K code, which implements a full-potential linear augmented plane-wave formalism [27]. We selected the generalized gradient approximation to represent exchange-correlation functional [28]. The hybridization expansion version continuous-time quantum Monte Carlo impurity solver (dubbed as CT-HYB) [29–31] was used to solve the quantum impurity model within the DMFT part. Undoubtedly, the 4f bands were treated as correlated orbitals. The corresponding interaction parameters were on-site Coulomb interaction  $U=6.0~{\rm eV}$  and Hund's coupling  $J=0.7~{\rm eV}$  [15, 16]. The experimental lattice structures and system temperature  $T\sim290~{\rm K}$  ( $\beta=40.0$ ) were used throughout the calculations.

### III. RESULTS

Momentum-resolved spectral functions  $A(\mathbf{k}, \omega)$ . The calculated band structures of the three high-pressure phases along the high-symmetry lines in the Brillouin zone are displayed in Fig. 2. Since most of the 4f bands in Ce are unoccupied, their positions are well above the Fermi level. As  $E_F < \omega < 1.5$  eV, we observe some intense and stripe-like features, which are mainly associated with the 4f bands. Their bandwidths are approximately  $0.8 \sim 1.2$  eV, which are much smaller than the Coulomb interaction strength (i.e.,  $W \ll U$ ). It is an exact evidence to support the statement that the 4f bands in the high-pressure phases of Ce are still strongly correlated [21]. In addition, we also observe heavy c - f hybridizations between the 4f and the spd conduction bands in this energy win-

dow. As  $\omega > 1.5$  eV and  $\omega < E_F$ , the general features become somewhat blurry. The bands in this energy range exhibit remarkable dispersions and large bandwidths. Apparently, they belong to the *spd* itinerant bands to a large extent.

Now let us concentrate on the similarities and differences in the band structures of the three phases. As for the  $\alpha'$  and  $\alpha''$  phases, since their lattice volumes are very close and their crystal structures are tightly related, the corresponding band structures are quite similar and share some common features, such as the positions of the 4f and valence bands. However, for the  $\epsilon$  phase, which exists under higher pressure and thus has a smaller lattice volume [9], the center of the correlated 4f bands shifts upwards slightly and the itinerant spd bands exhibit much more significant dispersions. Finally, from Fig. 2, we can speculate that for the  $\epsilon$  phase the volume encapsulated by the Fermi surface is the smallest. In the  $\alpha'$  and  $\alpha''$  phases, the Fermi surfaces that enclose the  $\Gamma$  point are hole-type and electron-type, respectively.

Density of states  $A(\omega)$ . The total density of states  $A(\omega)$  are shown in Fig. 3(a). In the vicinity of the Fermi level, there is the so-called Kondo resonance peak with sharp two-peak structure. This splitting is owing to the spin-orbit coupling effect. Away from the Fermi level, the spectrum spreads out and becomes almost featureless. Just as discussed above, the spectra for the  $\alpha'$  and  $\alpha''$  phases are very similar, including the magnitude of the Kondo resonance peak, the two satellite peaks between -2 eV and  $E_F$ , and the total bandwidth. As for the  $\epsilon$  phase, its spectrum turns broader and has a stronger Kondo resonance peak.

The 4f partial density of states  $A_{4f}(\omega)$  are shown in Fig. 3(b). Clearly, according to the difference between  $A(\omega)$ and  $A_{4f}(\omega)$ , the contributions from the 4f bands are predominant near the Fermi level. They compose the Kondo resonance peak. On the other hand, below the Fermi level, the itinerant spd bands are the most important (the 4f spectral weight approaches zero). Due to the spin-orbit coupling, the 4f bands are split into two components, namely  $4f_{5/2}$  and  $4f_{7/2}$ . The  $4f_{5/2}$  component has a lower energy and is closer to the Fermi level. The lower Hubbard bands are almost invisible since the 4f occupancy is small. The upper Hubbard bands look like broad "humps", and they locate roughly from 2 eV to 8 eV. All these features are comparable to those already found in the  $\alpha$  phase by using the DFT + DMFT method [14–17] and photoemission spectroscopy [32, 33]. Compared to the  $\alpha'$  and  $\alpha''$  phases, the  $A_{4f}(\omega)$  of the  $\epsilon$  phase is a bit different. The peaks ascribed to the  $4f_{5/2}$  and  $4f_{7/2}$  components (and the upper Hubbard bands) have larger intensity, and their positions are shifted to high-energy regime marginally.

In Fig. 3(c), we visualize the imaginary parts of the real-frequency hybridization functions, i.e.,  $-\Im\Delta(\omega)/\pi$ , which are approximately proportional to the strength of hybridization effect between the strongly correlated 4f bands and the weakly correlated (or non-correlated) spd bands. We can see that the hybridization effect is very strong, especially near the Fermi level. It indicates that the KVC scenario not only can be used to explain the  $\alpha-\gamma$  phase transition [4, 5], but also is useful for understanding the underlying electronic structures of the high-pressure phases of Ce. Noticed that the hybridization function

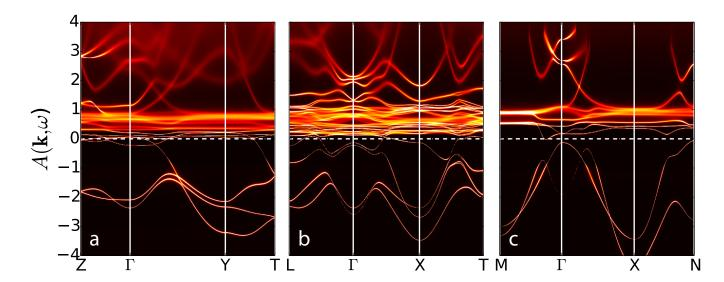


FIG. 2. (Color online). Momentum-resolved spectral functions  $A(\mathbf{k}, \omega)$  of Ce under high pressure. (a)  $\alpha'$ -Ce. (b)  $\alpha''$ -Ce. (c)  $\epsilon$ -Ce. They were calculated via the analytical continuation of Matsubara self-energy function [26]. The horizontal dashed lines represent the Fermi level.

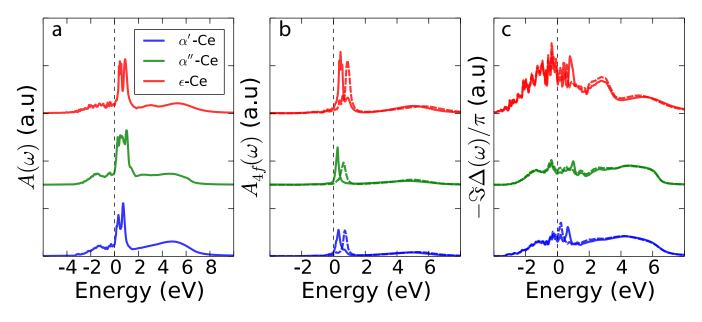


FIG. 3. (Color online). (a) Total density of states  $A(\omega)$ , (b) 4f partial density of states  $A_{4f}(\omega)$ , and (c) 4f hybridization functions  $-\Im\Delta(\omega)/\pi$  of Ce under high pressure. They were calculated via the analytical continuation of Matsubara self-energy function [26]. The data are rescaled and shifted vertically for a better view. In panels (b) and (c), the spectra for the  $4f_{5/2}$  and  $4f_{7/2}$  components are plotted as solid and dashed lines, respectively. The vertical dashed lines represent the Fermi level.

of the  $\epsilon$  phase is much higher than the others, which implies that its 4f electrons tend to be more itinerant. Naturally, we believe that the valence state fluctuation in the  $\epsilon$  phase must be the most pronounced among cerium's allotropes. We will discuss this issue later.

Distribution of atomic eigenstates. The CT-HYB quantum impurity solver is capable of computing the valence state histogram  $p_{\Gamma}$ , which means the probability to find a valence state electron (such as the 4f electrons in Ce) in a given atomic eigenstate  $|\psi\rangle$  (labelled by  $\Gamma$ ) [30]. It provides us a powerful

lens to learn the subtle electronic structures of strongly correlated systems directly. Besides the first successful application for the 4f electrons in  $\alpha$  and  $\gamma$ -Ce, it has been adopted to analyze the status of 5f electrons in  $\alpha$  and  $\delta$ -Pu [24, 25], and the 4f localized-itinerant crossover in heavy fermion compound CeIn $_3$  [34]. Here, we would like to utilize it to unveil whether the 4f electrons in the high-pressure phases of Ce are localized or not. In the presence of spin-orbit coupling, the 4f atomic eigenstates could be classified by using the good quantum numbers N (total occupancy) and J (total

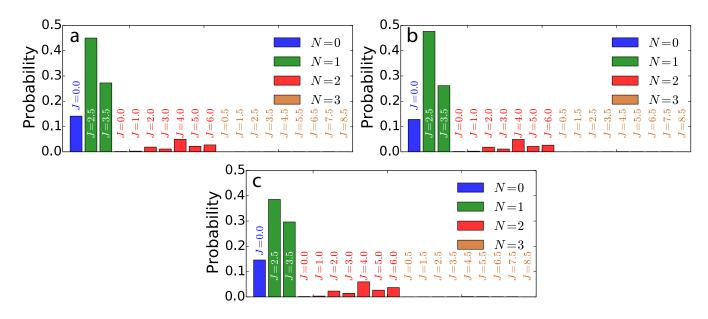


FIG. 4. (Color online). Probabilities of the 4f atomic eigenstates (or equivalently valence state histograms) of Ce under high pressure. (a)  $\alpha'$ -Ce. (b)  $\alpha''$ -Ce. (c)  $\epsilon$ -Ce. Note that the histograms from the N=3 atomic eigenstates are too trivial to be seen in this figure.

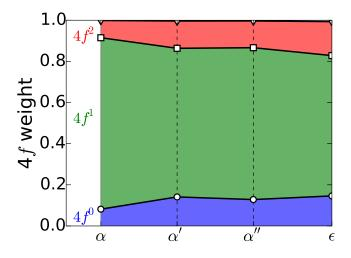


FIG. 5. (Color online). Distributions of 4f electronic configurations of  $\alpha$ ,  $\alpha'$ ,  $\alpha''$ , and  $\epsilon$ -Ce.

angular momentum). In the present work, in order to accelerate the calculations, we made a crucial truncation that only those atomic eigenstates whose  $N \in [0,3]$  were taken into considerations [30]. Next we will prove that the contributions from the atomic eigenstates with larger occupancy  $(N \ge 3)$  are trivial and the truncation we used is reasonable.

The calculated valence state histograms are shown in Fig. 4. As is seen in this figure, the predominant atomic eigenstates are  $|N=1,J=2.5\rangle$  and  $|N=1,J=3.5\rangle$ . Their probabilities add up to about  $68\% \sim 74\%$ . The less important atomic eigenstate is  $|N=0,J=0.0\rangle$ , which amounts to about  $13\% \sim 15\%$ . For the N=2 case, the contributions from various atomic eigenstates account for about  $13\% \sim 17\%$ . They are comparable and no dominant ones. The probabilities for the

atomic eigenstates with N=3 are tiny (< 1% in total), so it is hardly to see them in Fig. 4. Since the contributions from the  $N \geq 3$  atomic eigenstates are unimportant, it is acceptable to discard them to improve the efficiency during the DFT + DMFT calculations. Actually, we rerun all of the calculations with  $N \in [0,2]$  and  $N \in [0,4]$ . The calculated results are practically identical.

Next, let us compare the valence state histograms of the three phases. First, in the  $\alpha'$  and  $\alpha''$  phases, the probability of the  $|N=1,J=2.5\rangle$  eigenstate is nearly twice as much as the one of the  $|N=1,J=3.5\rangle$  eigenstate. While for the  $\epsilon$  phase, the probabilities for the two atomic eigenstates are close. Second, the probabilities for the N=0,2, and 3 cases in the  $\epsilon$  phase are somewhat larger than those in the  $\alpha'$  and  $\alpha''$  phases. All these facts reveal that the 4f electrons in the high-pressure phases of cerium are not always bound to the N=1 case, and tend to hop among a variety of atomic eigenstates with different occupancy and angular momentum. Especially for the  $\epsilon$  phase, this tendency is the most noticeable.

Valence state fluctuations. From the 4f valence state histograms, we can easily evaluate the distributions of 4f electronic configurations, and then discuss the valence state fluctuation phenomenon which usually manifests itself in the rare earth compounds (such as the Ce-based, Sm-based, and Yb-based heavy fermion systems [23, 35]) and the actinides (such as Pu [24, 25]). Supposed that the weight for the  $4f^i$  (where  $i \in [0,3]$ ) configuration is  $W(4f^i)$ , then it can be calculated via the following equation,

$$W(4f^{i}) = \sum_{N} \sum_{I} \delta(N - i) p_{\Gamma}. \tag{1}$$

We tried to calculate the weights for the  $4f^{[0-3]}$  electronic configurations. The results are presented in Fig. 5. In order to gain a clear impression about the evolution of electronic

configurations, we performed additional calculations for the  $\alpha$  phase, and supplemented its data to this figure. Obviously, for  $\mathcal{W}(4f^1)$ , we have  $\alpha > \alpha' \approx \alpha'' > \epsilon$ . However, for  $\mathcal{W}(4f^0)$  or  $\mathcal{W}(4f^2)$ , the sequence is inverse, i.e.,  $\alpha < \alpha' \approx \alpha'' < \epsilon$ .

Based on the obtained data, we reached the following conclusions. First, the distributions of electronic configurations for the  $\alpha'$  and  $\alpha''$  phases are similar in all respects. Second, in the high-pressure phases of cerium, the 4f valence state fluctuations are more significant than the phases under ambient pressure. Particularly, in the  $\epsilon$  phase, the 4f valence state fluctuation is much stronger than the other allotropes. Third, strong valence state fluctuation will modify the valence state occupancy inevitably. Thus we employed the following equation to evaluate the averaged 4f occupancy  $N_{4f}$  [34],

$$N_{4f} \approx \sum_{i=0}^{3} \mathcal{W}(4f^{i}) \times i. \tag{2}$$

The calculations suggest that the  $N_{4f}$  for the  $\alpha'$ ,  $\alpha''$ , and  $\epsilon$  phases are 0.98, 0.99, and 1.03, respectively [36]. Alternatively, the 4f occupancy is only modified slightly in this case.

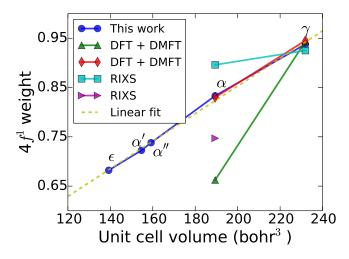


FIG. 6. (Color online). The  $4f^1$  weight  $\mathcal{W}(4f^1)$  with respect to the unit cell volumes V [37] of various phases of Ce. The DFT + DMFT data for reference are extracted from Reference [30] (upper triangle symbols) and [16] (diamond symbols). The resonant inelastic X-Ray scattering (RIXS) experimental data for  $\alpha$ -Ce and  $\gamma$ -Ce are taken from Reference [38]. For  $\alpha$ -Ce, the data were measured under 10 kbar (square symbol) and 20 kbar (right triangle symbol). For  $\gamma$ -Ce, the data were measured under 0 kbar (square symbol). See main text for the detailed explanations.

Discussions. Under external pressure, the unit cell volumes

of cerium is reduced, and the corresponding electronic structure (including the band structure, density of states, Fermi surface, valence state histogram, and distribution of electronic configuration) is tuned gradually. Here, we would like to figure out the relationship between the lattice volume and the 4f electronic configurations.

In Fig. 6, we try to plot the  $W(4f^1)$  against lattice volume [37]. Besides the three high-pressure phases, the available data for the  $\alpha$  and  $\gamma$  phases are also included. Surprisingly, we find that the  $W(4f^1) - V$  curve exhibits a quasilinear behavior. Then we used the formula f(x) = ax + b to fit the data (please see the dashed dark-yellow line in Fig. 6). The fitting parameters a and b are 0.00279767 and 0.293449, respectively. This linear behavior is easily to be understood. The larger the lattice volume is, the more localized the 4felectrons are, and the smaller the 4f valence state fluctuation will be. As a result, the 4f electrons have a tendency to stay at the  $4f^1$  electronic configuration instead of hopping to and fro, with respect to the increment of lattice volume. On the other hand, we think that the  $W(4f^1)$  could be considered as a quantitative tool to measure the valence state fluctuation and electronic localized degree of freedom for Ce-based system.

### IV. SUMMARY

In conclusion, we studied the electronic structures of three high-pressure phases of Ce by using the charge fully self-consistent DFT + DMFT method. We found that the 4f electrons exhibit more itinerant features. And the valence state fluctuation in the  $\epsilon$  phase is the most remarkable, which is precisely described by the quantity  $W(4f^1)$ . To the best of our knowledge, it is the first time to adopt the first-principles many-body approach to study the  $\alpha'$ ,  $\alpha''$ , and  $\epsilon$ -Ce. It is also the first step to build an unified picture for the electronic structures and related physical properties of all allotropes of Ce. Unfortunately, the corresponding experiments are rare in the literatures. Our results serve as critical predictions, and require further experimental examinations.

## ACKNOWLEDGMENTS

This work was supported by the Natural Science Foundation of China (No. 11504340), the Foundation of President of China Academy of Engineering Physics (No. YZ2015012), the Discipline Development Fund Project of Science and Technology on Surface Physics and Chemistry Laboratory (No. 201502), and the Science Challenge Project of China (No. JCKY2016212A56401).

<sup>[1]</sup> David C. Koskenmaki and Karl A. Gschneidner Jr., in *Handbook on the Physics and Chemistry of Rare Earths*, Vol. 1, edited by Karl A. Gschneidner Jr. and LeRoy Eyring (Elsevier, 1978) Chap. 4.

<sup>[2]</sup> B. Johansson, Phil. Mag. 30, 469 (1974).

<sup>[3]</sup> B. Johansson, I. A. Abrikosov, M. Aldén, A. V. Ruban, and H. L. Skriver, Phys. Rev. Lett. 74, 2335 (1995).

<sup>[4]</sup> J. W. Allen and R. M. Martin, Phys. Rev. Lett. 49, 1106 (1982).

- [5] J. W. Allen and L. Z. Liu, Phys. Rev. B 46, 5047 (1992).
- [6] I.-K. Jeong, T. W. Darling, M. J. Graf, T. Proffen, R. H. Heffner, Y. Lee, T. Vogt, and J. D. Jorgensen, Phys. Rev. Lett. 92, 105702 (2004).
- [7] M. J. Lipp, D. Jackson, H. Cynn, C. Aracne, W. J. Evans, and A. K. McMahan, Phys. Rev. Lett. 101, 165703 (2008).
- [8] T. Jarlborg, Phys. Rev. B 89, 184426 (2014).
- [9] A. V. Nikolaev and A. V. Tsvyashchenko, Physics-Uspekhi 55, 657 (2012).
- [10] I. Loa, E. I. Isaev, M. I. McMahon, D. Y. Kim, B. Johansson, A. Bosak, and M. Krisch, Phys. Rev. Lett. 108, 045502 (2012).
- [11] F. H. Ellinger and W. H. Zachariasen, Phys. Rev. Lett. **32**, 773
- [12] J. Smith and E. Kmetko, J. Less Common Metals 90, 83 (1983).
- [13] K. Haule, V. Oudovenko, S. Y. Savrasov, and G. Kotliar, Phys. Rev. Lett. 94, 036401 (2005).
- [14] A. K. McMahan, K. Held, and R. T. Scalettar, Phys. Rev. B 67, 075108 (2003).
- [15] K. Held, A. K. McMahan, and R. T. Scalettar, Phys. Rev. Lett. 87, 276404 (2001).
- [16] M. B. Zölfl, I. A. Nekrasov, T. Pruschke, V. I. Anisimov, and J. Keller, Phys. Rev. Lett. 87, 276403 (2001).
- [17] A. K. McMahan, Phys. Rev. B 72, 115125 (2005).
- [18] B. Amadon, S. Biermann, A. Georges, and F. Aryasetiawan, Phys. Rev. Lett. 96, 066402 (2006).
- [19] B. Chakrabarti, M. E. Pezzoli, G. Sordi, K. Haule, and G. Kotliar, Phys. Rev. B 89, 125113 (2014).
- [20] G. Kotliar, S. Y. Savrasov, K. Haule, V. S. Oudovenko, O. Parcollet, and C. A. Marianetti, Rev. Mod. Phys. 78, 865 (2006).
- [21] A. Georges, G. Kotliar, W. Krauth, and M. J. Rozenberg, Rev. Mod. Phys. 68, 13 (1996).
- [22] J. A. Mydosh and P. M. Oppeneer, Rev. Mod. Phys. 83, 1301 (2011).
- [23] E. R. Ylvisaker, J. Kuneš, A. K. McMahan, and W. E. Pickett, Phys. Rev. Lett. 102, 246401 (2009).

- [24] J. H. Shim, K. Haule, and G. Kotliar, Nature 446, 513 (2007).
- [25] M. Janoschek, P. Das, B. Chakrabarti, D. L. Abernathy, M. D. Lumsden, J. M. Lawrence, J. D. Thompson, G. H. Lander, J. N. Mitchell, S. Richmond, M. Ramos, F. Trouw, J.-X. Zhu, K. Haule, G. Kotliar, and E. D. Bauer, Sci. Adv. 1, 1500188 (2015).
- [26] K. Haule, C.-H. Yee, and K. Kim, Phys. Rev. B 81, 195107 (2010).
- [27] P. Blaha, K. Schwarz, G. Madsen, D. Kvasnicka, and J. Luitz, WIEN2k, An Augmented Plane Wave + Local Orbitals Program for Calculating Crystal Properties (Karlheinz Schwarz, Techn. Universitt Wien, Austria, 2001).
- [28] J. P. Perdew, K. Burke, and M. Ernzerhof, Phys. Rev. Lett. 77, 3865 (1996).
- [29] E. Gull, A. J. Millis, A. I. Lichtenstein, A. N. Rubtsov, M. Troyer, and P. Werner, Rev. Mod. Phys. 83, 349 (2011).
- [30] K. Haule, Phys. Rev. B 75, 155113 (2007).
- [31] P. Werner, A. Comanac, L. de' Medici, M. Troyer, and A. J. Millis, Phys. Rev. Lett. 97, 076405 (2006).
- [32] D. M. Wieliczka, C. G. Olson, and D. W. Lynch, Phys. Rev. B 29, 3028 (1984).
- [33] E. Wuilloud, H. R. Moser, W. D. Schneider, and Y. Baer, Phys. Rev. B 28, 7354 (1983).
- [34] H. Lu and L. Huang, Phys. Rev. B 94, 075132 (2016).
- [35] I. Jarrige, H. Yamaoka, J.-P. Rueff, J.-F. Lin, M. Taguchi, N. Hiraoka, H. Ishii, K. D. Tsuei, K. Imura, T. Matsumura, A. Ochiai, H. S. Suzuki, and A. Kotani, Phys. Rev. B 87, 115107 (2013).
- [36] We can evaluate the 4f occupations  $N_{4f}$  through the impurity Green's function  $G(\tau)$  or  $G(i\omega_n)$ , but usually the calculated values are a little smaller.
- [37] Here, the volume means the lattice volume occupied by single cerium atom.
- [38] J.-P. Rueff, J.-P. Itié, M. Taguchi, C. F. Hague, J.-M. Mariot, R. Delaunay, J.-P. Kappler, and N. Jaouen, Phys. Rev. Lett. 96, 237403 (2006).